Probing the Low-Temperature Water−Gas Shift Activity of Alkali-Promoted Platinum Catalysts Stabilized on Carbon Supports

Branko Zugic,[†] Shiran Zhang,[‡] David C. Bell,[§] Franklin (Feng) Tao,[‡] and Maria Flytzani-Stephanopoulos*,[†]

[†]Department of Chemical and Biological Engineering, Tufts University, Medford, Massachusetts 02155, United States
[‡]Department of Chemistry and Biochemistry, Notre Dame University, Notre Dame Indiana 46556, United States
[§]School of Engineering and Applied Sciences, Harvard University, Cambridge, Massachusetts 02138, United States

ⓢ *Supporting Information*

ABSTRACT: We report on the direct promotional effect of sodium on the water−gas shift activity of platinum supported on oxygen-free multiwalled carbon nanotubes. Whereas the Na-free Pt catalysts are shown to be completely inactive, the addition of sodium is found to improve the water−gas shift activity to levels comparable to those obtained with highly active Pt catalysts on metal oxide supports. The structure and morphology of the catalyst surface was followed using aberration-corrected HAADF-STEM, which showed that atomically dispersed platinum species are stabilized by the addition of sodium. In situ atmospheric-pressure X-ray photoelectron spectroscopy (AP-XPS) experiments demonstrated that oxidized platinum Pt−OH$_x$ contributions in the Pt 4f signal are higher in the presence of sodium, providing evidence for a previously reported active-site structure of the form Pt−Na$_x$−O$_y$−(OH)$_z$. Pt remained oxidized in all redox experiments, even when a H$_2$-rich gas mixture was used, but the extent of its oxidation followed the oxidation potential of the gas. These findings offer new insights into the nature of the active platinum-based site for the water−gas shift reaction. A strong inhibitory effect of hydrogen was observed on the reaction kinetics, effectively raising the apparent activation energy from 70 ± 5 kJ/mol (in product-free gas) to 105 ± 7 kJ/mol (in full reformate gas). Increased hydrogen uptake was observed on these materials when both Pt and Na were present on the catalyst, suggesting that hydrogen desorption might limit the water−gas shift reaction rate under such conditions.
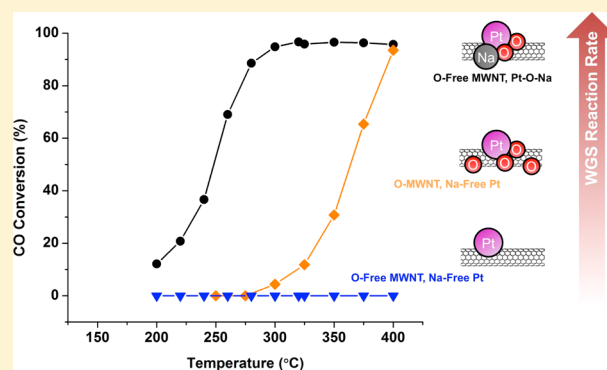
INTRODUCTION

The water−gas shift (WGS) reaction is an essential step in the purification process for on-board fuel reforming and hydrogen production. It is of particular importance for low-temperature polymer electrolyte membrane (PEM) fuel cell applications, where CO levels must be decreased to <1 ppm at relatively low temperatures to prevent poisoning of the anode catalysts.[1] The current industrial Cu−ZnO-based low-temperature WGS catalysts are not well-suited for this process because of their pyrophoricity and susceptibility to deactivation under ambient conditions. As such, attention has recently turned to advanced copper-based catalysts[2−4] and a new generation of noble-metal catalysts[5−8] in an effort to find suitable alternatives.

Platinum has been of particular interest as an alternative WGS catalyst owing to its high WGS activity and resistance to poisoning.[9] As a result of the considerable progress made in the area of automotive exhaust catalysis, significant improvements in our understanding of how platinum catalyzes the water−gas shift reaction at low temperatures have been made, especially on ceria and doped-ceria supports.[5,6,8,10−14] This topic has recently been reviewed.[15,16] A bifunctional mechanism has been inferred in the literature on the subject, in which the support oxide activates water as CO is adsorbed on Pt.[17] For Pt surfaces, the concentration of hydroxyl groups has been shown to control the rate of the WGS reaction[14] and is therefore indispensable for high CO conversions. Accordingly, the activity of ceria-supported catalysts is attributed to the high oxygen defect concentrations in this support,[5,8,11,13,18] leading to a high rate of water activation to surface hydroxyl groups and, in turn, to high WGS activity.

The active site on these materials has been identified as oxidized platinum present as Pt−O$_x$−Ce species on the surface.[5,19] The strong interaction created by this structure gives the catalyst improved stability (i.e., resistance to sintering)[19] and makes ceria the support of choice for Pt as well as other active metals such as gold[5,20−22] and copper.[4,23] At low temperatures, however, ceria itself is susceptible to deactivation due to hydroxycarbonate formation, which can be overcome by using O$_2$-assisted WGS conditions[13] or by

doping ceria with additives (i.e., zirconia).[12] It is therefore fair to say that the search for improved low-temperature shift catalysts has continued unabated over the years.

It was recently reported that the addition of alkali metals to platinum supported on metal oxide supports promotes its activity.[24−29] Furthermore, Pt was shown to be promoted by alkali metal oxides even on inert supports such as silica; the resulting catalysts have comparable activity and improved stability when compared to Pt/CeO_2.[27,29] Using ab initio molecular dynamics to match the reactivity and spectroscopic characterization data, plausible clusters centered on Pt ligated to alkali atoms through oxygen and containing some number of −OH species were proposed[27] (the Pt atom is positively charged in such clusters). We recently reported that Pt can be promoted by Na even when deposited on multiwalled carbon nanotubes (MWNTs).[30] The presence of oxygen-containing groups on the surface of the carbon was shown to strongly affect the stability of the oxidized platinum species in such catalysts.

In an effort to understand whether this active site is common across all supports, we have chosen here an inert, oxygen-free carbon material as the support for the $Pt−Na_x−O_y−(OH)_z$ clusters. These catalysts were characterized under reaction conditions using ambient-pressure X-ray photoelectron spectroscopy (AP-XPS)[31,32] to provide new insights into the nature of adsorbed species and their effects on the active Pt sites. Carbon-supported Pt catalysts have historically been avoided in the study of the WGS reaction because of their low activity.[17] However, the stability and activity that Na imparts to the Pt catalyst provides a means of accurately monitoring platinum *and* oxygen changes on the carbon-based surface because of the low contributions from the bulk (i.e., support) oxygen.

We show here that the activity and stability of Pt deposited on annealed (oxygen-free) MWNTs are strongly promoted by the addition of sodium. Characterization by atomic-resolution microscopy and AP-XPS demonstrates the presence of highly dispersed $Pt−OH_x$ species on alkali-promoted Pt catalysts. In addition to steady-state activity tests, dynamic reactivity studies are used to further elucidate the properties of the $Pt−O_x−Na_y−OH_z$ active site for the WGS reaction.

■ EXPERIMENTAL SECTION

Multiwalled carbon nanotubes (>95%, o.d. 20−30 nm, length 10−30 μm) were purchased from Cheap Tubes, Inc. Purification and introduction of surface oxygen was performed by nitric acid oxidation. The as-received MWNTs (denoted C_N) were suspended in 70% HNO_3 (Alfa Aesar) (25 mL per gram of MWNTs) and refluxed at 120 °C for 2 h (denoted 2h-C_N). After being refluxed, the oxidized MWNTs were filtered and washed repeatedly with deionized water until neutral pH was observed in the filtrate. The washed nanotubes were placed in a vacuum oven and dried overnight at 60 °C. They were then annealed at 1000 °C for 4 h under flowing helium to remove all surface oxygen (denoted 1000-2h-C_N).

Platinum-containing catalysts (1 wt % Pt) were prepared by incipient wetness impregnation of the as-received and treated MWNTs using a tetraamine platinum nitrate (Sigma-Aldrich) precursor dissolved in the appropriate amount of water (C_N pore volume = 1.5 mL/g). SiO_2-supported catalysts were prepared using fumed silica (Sigma-Aldrich, pore volume = 3 mL/min). For the sodium-promoted catalysts, sodium nitrate (Alfa Aesar) was added to the impregnation solution to give a 6:1 molar ratio of Na to Pt. Following impregnation, the MWNT-supported catalysts were dried in a vacuum and annealed in flowing helium at 400 °C for 1 h.

Steady-state WGS activity tests were performed in a packed-bed quartz reactor operated at atmospheric pressure. The feed and product

gas compositions were analyzed using an SRI 331 gas chromatograph (GC) equipped with a Carbosphere 80/100 packed column and a thermal conductivity detector (TCD). In a typical experiment, 0.1−0.2 g of catalyst was diluted with calcined quartz sand and loaded between two plugs of quartz wool. The gas composition for product-free activity tests was 2% CO/10% H_2O/88% He, using a flow rate of 70 mL/min. Full reformate gas tests were performed using a gas mixture of 11% CO/25% H_2/25% H_2O/7% CO_2/32% He at flow rates of 150−210 mL/min. The samples were first exposed to the full gas composition at 350 °C for 2 h and 300 °C for 48 h before the kinetic tests were performed under full reformate gas conditions. The CO conversion was kept below 15% during the kinetic tests. Methane production was not observed under any of the WGS reaction conditions used.

H_2 temperature-programmed desorption (TPD) experiments were performed using a Micromeritics AutoChem 2920 II apparatus. In a typical experiment, 0.1 g of catalyst was placed in a U-shaped quartz reactor between two plugs of quartz wool. The catalysts were prereduced in 10% H_2/Ar at 400 °C (10 °C/min) and then cooled to room temperature and purged in He. The temperature was then ramped to 400 °C in flowing He (30 mL/min) at 10 °C/min, and the effluent gas was monitored by a residual gas analyzer (SRS RGA 200).

Aberration-corrected (ac) high-angle annular dark-field scanning transmission electron microscopy (HAADF-STEM) imaging was performed using a Zeiss Libra 200 MC microscope operated at 200 kV. Samples were prepared by dispersing the powders in ethanol and dropping the resulting solutions onto a 200-mesh copper grid coated with a lacey carbon film. Particle sizes were estimated from the images by counting at least 300 particles.

Ambient-pressure X-ray photoelectron spectroscopy (AP-XPS) was performed using an in-house spectrometer[31,32] equipped with a benchtop monochromated Al Kα source, a reaction cell, and a series of differential pumping stages leading to the analyzer. Samples were mounted on a highly oriented pyrolytic graphite (HOPG) substrate and placed into the sample holder. Reactions were performed under ultrahigh vacuum (UHV) at varying reaction conditions (0.1 mbar of CO, 0.5 mbar of H_2O, 0.5 mbar of H_2, and combinations thereof) and various temperatures (25−350 °C). The samples were heated conductively through an external heating source installed in the UHV chamber to eliminate the influence of a filament. Reactant gas was allowed to flow through the reaction cell during XPS analysis, while the sample was kept at a maximum distance of 0.3 mm from the aperture of the analyzer to ensure a spacing smaller than the inelastic mean free path of photoelectrons of 500 eV in the corresponding gaseous environment. The presence of gas-phase CO_2 contributions at 536.3 eV (in addition to CO and H_2O at 538.0 and 535.4 eV, respectively) in the O 1s signal at elevated temperatures when the Na-promoted catalyst was used indicated that XP spectra were collected under representative reaction (i.e., CO conversion) conditions.

The deconvolution of AP-XP spectra was performed using the CasaXPS analysis software suite. Gaussian (70%)/Lorentzian (30%) peak shapes were used for all components. The binding energy and full width at half-maximum (fwhm) were fixed for each component (determined using UHV and room-temperature scans) and maintained throughout all fits. The variability for all binding-energy and fwhm values was kept below ±0.1.

The initial Pt 4f UHV spectra of both the Na-promoted and unpromoted catalysts were fitted using known peak positions[33] for Pt^0 (71.4 eV), Pt^{1+}/Pt−OH (72.4 eV), Pt^{2+} (74.1 eV), and Pt^{4+} (74.9 eV), with the fwhm set to 1.2 for Pt^0, 1.5 for Pt^{1+}, 1.5 for Pt^{2+}, and 1.5 for Pt^{4+}. Upon the addition of CO to the gas phase at room temperature, the peaks corresponding to CO bound to Pt in top and bridge positions (72 eV with 0.9 fwhm) and CO bound to low-coordinated Pt sites (72.7 eV with 0.9 fwhm)[34−36] were added. All fitting was performed using the Marquardt algorithm.

■ RESULTS AND DISCUSSION

Catalyst Activity Studies. The water−gas shift (WGS) activity of the Na-promoted and unpromoted Pt catalysts under

product-free conditions are shown in Figure 1. The CO conversion for the 1 wt % Pt/C_N catalyst (prepared on as-
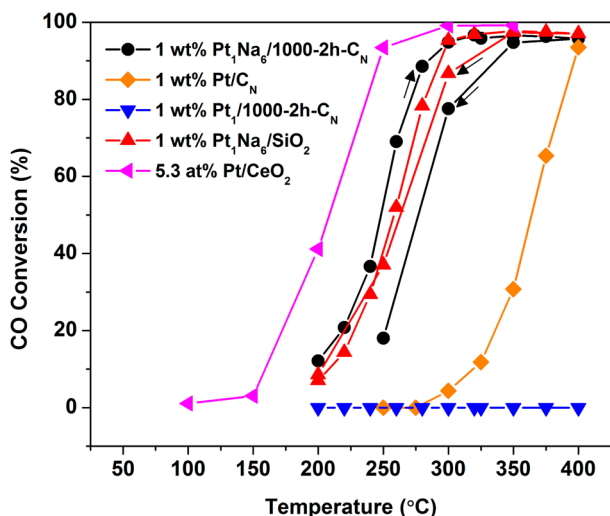

Figure 1. Steady-state WGS activity of Pt catalysts prepared on untreated (Pt/C_N) and acid-treated/annealed ($Pt/1000\text{-}2h\text{-}C_N$) supports in the absence of Na and the corresponding sodium-promoted ($Pt_1Na_6/1000\text{-}2h\text{-}C_N$) catalyst. Results for the Na-promoted catalyst on SiO_2 (Pt_1Na_6/SiO_2) and a 5 wt % Pt/CeO_2 catalyst are shown for comparison. Conditions: 70 mL/min 2% CO/10% H_2O/88% He, 0.1 g of catalyst.

received MWNTs) was observed to light off around 275 °C and approach full conversion at 400 °C. In addition to the 1 wt % Pt/C_N catalyst, platinum was also deposited on carbon nanotubes that were purified/oxidized by HNO_3 treatment and annealed at 1000 °C in flowing helium to completely remove surface oxygen functionality, labeled 1 wt % Pt/1000-2h-C_N. Interestingly, this catalyst did not show any activity for the WGS reaction in the temperature range of 200–400 °C. This can be explained by the lack of surface sites that are able to activate (i.e., dissociate) water molecules. Indeed, previous reports have shown the formation of hydroxyl groups to be key for WGS activity.[14,27,37] On the as-received nanotubes (C_N), significant amounts of functional groups, including carboxylic and hydroxyl groups, are present (see Figure S1, Supporting Information) on the surface. These groups act to anchor and disperse Pt as well as activate water, thus explaining the measurable WGS reaction activity (at >275 °C) of the 1 wt % Pt/C_N catalyst shown in Figure 1.

The coimpregnation of Pt and Na on the annealed nanotubes (labeled 1 wt % $Pt_1Na_6/1000\text{-}2h\text{-}C_N$) resulted in a catalyst of high WGS activity (Figure 1). This is in line with previous reports that have shown sodium to have a strong promotional effect on metal-oxide-supported Pt catalysts.[24,25,27−30,38] However, the current finding of high WGS activity over Pt supported on an oxygen-free (MWNT) surface corroborates the ability of sodium (oxide) alone to interact with platinum and provide sites for water activation. This is of particular importance, as metal oxide supports are typically thought to play the essential role of dissociating H_2O in the WGS mechanism on highly active Pt catalysts[5,6,39,40] (e.g., Pt/CeO_2; the CO conversion on a 5 wt % Pt/CeO_2 sample is also shown in Figure 1 for comparison[6]). In fact, the 1 wt % $Pt_1Na_6/1000\text{-}2h\text{-}C_N$ catalyst prepared in this study was observed to have nearly identical WGS activity to the analogous sodium-

ion-promoted platinum catalyst prepared on fumed silica (i.e., 1 wt % Pt_1Na_6/SiO_2[27] in Figure 1). Furthermore, the apparent activation energy for the WGS reaction on $Pt_1Na_6/1000\text{-}2h\text{-}C_N$, calculated from the low-conversion points in Figure 1, is 70 ± 5 kJ/mol, in accordance with the values observed on other alkali-promoted Pt catalysts on various supports.[14,17,24,27−29,41] Hence, the sodium oxide can be considered as a "ceria analogue" in activating the platinum both on inert oxide surfaces[27,29] and on oxygen-free carbon. It is important to note here that the surface oxygen content of the annealed multiwalled carbon nanotubes (as measured by XPS; Table S1, Supporting Information) did not increase significantly (from 0.7 to 0.9 at. %) after the addition of Pt and Na.

ac-HAADF-STEM images of the fresh catalysts (after calcination in flowing He at 400 °C for 1 h) are shown in Figure 2. It can be seen from the images and the particle size
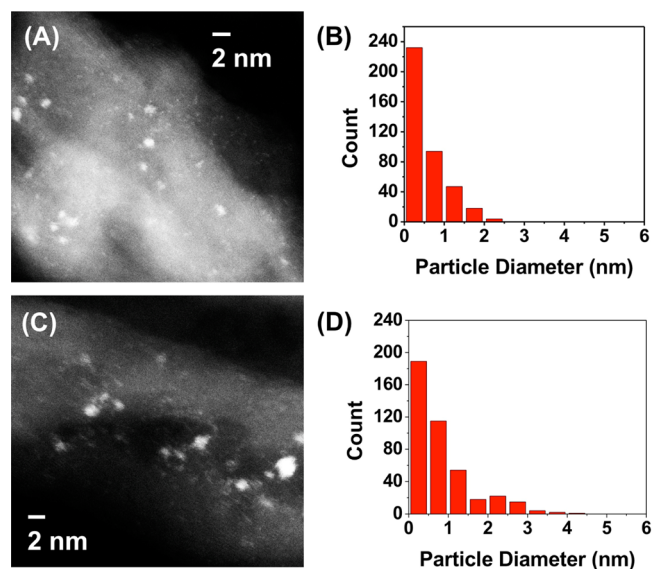

Figure 2. (A,C) Aberration-corrected HAADF-STEM images and (B,D) corresponding particle size distributions of fresh (A,B) 1 wt % Pt/1000-2h-C_N and (C,D) 1 wt % $Pt_1Na_6/1000\text{-}2h\text{-}C_N$ catalysts.

distributions that very well-dispersed platinum clusters can be prepared on the carbon nanotubes with or without the addition of sodium. In both of these materials, more than 70% of the counted Pt particles were found to be smaller than 1 nm in diameter. After use in the WGS reaction, however, the average particle size of the Na-free catalyst increased to 1.7 nm, whereas that of the Na-promoted catalyst remained below 1 nm (Figure 3). From the ac-HAADF-STEM image and particle size distribution of $Pt_1Na_6/1000\text{-}2h\text{-}C_N$ in Figure 2C,D, it can be seen that 50% of the Pt on the Na-promoted support remained atomically dispersed below 1 nm.

The 1 wt % $Pt_1Na_6/1000\text{-}2h\text{-}C_N$ catalyst was also tested in a full reformate gas feed. The apparent activation energy (E_{app}) was found to increase from 70 ± 5 kJ/mol (in a product-free gas feed) to 105 ± 7 kJ/mol (in a full reformate gas feed) within the temperature range of 200–280 °C, as shown in the Arrhenius-type plot in Figure 4. We identified the cause of this inhibition of the WGS rate to be the presence of hydrogen in the reaction gas. Such an increase in the apparent activation energy has not been observed on alumina- or silica-supported Pt–Na catalysts,[27,29] except in one study that reported activation energies as high as 89 kJ/mol for very high alkali-
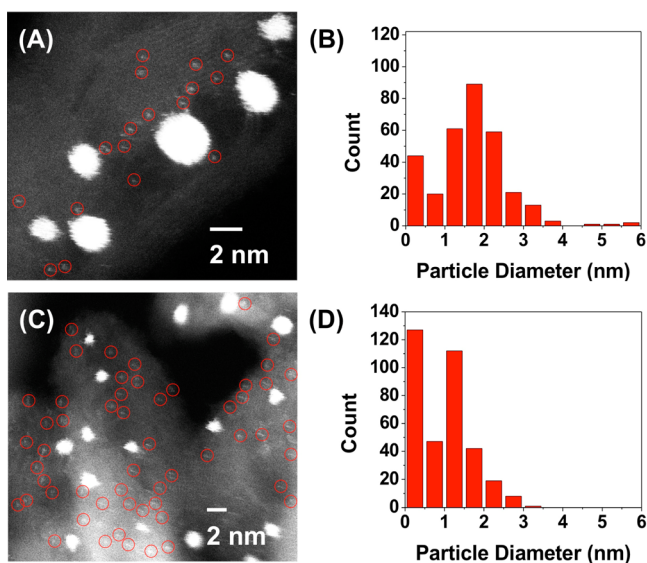
Figure 3. (A,C) Aberration-corrected HAADF-STEM images and (B,D) corresponding particle size distributions of used (conditions in Figure 1) (A,B) 1 wt% Pt/1000-2h-C_N and (C,D) 1 wt % Pt$_1$Na$_6$/1000-2h-C_N catalysts. Atomically dispersed species are circled in red.
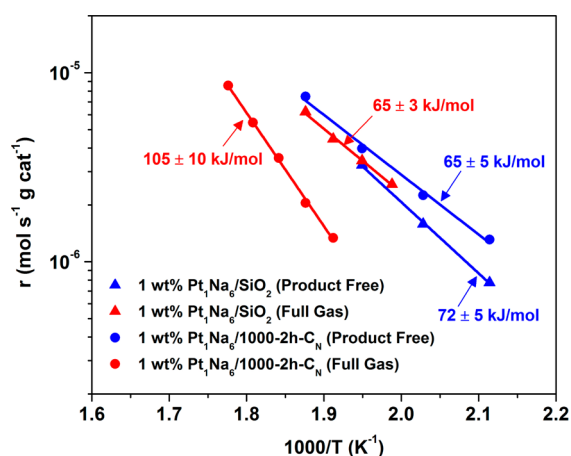

Figure 4. Arrhenius-type plot of Pt$_1$Na$_6$/1000-2h-C_N and Pt$_1$Na$_6$/SiO$_2$ in product-free (2% CO/10% H$_2$O/88% He) and full reformate gas (11% CO/25% H$_2$O/25% H$_2$/7% CO$_2$/32% He) conditions.

to-platinum ratios (e.g., 60:1) on Pt/Al$_2$O$_3$ catalysts.[28] This behavior, therefore, appears to be unique to the carbon-based catalysts examined here.

For comparison, an analogous Pt$_1$Na$_6$/SiO$_2$ catalyst (1 wt % Pt; Na/Pt = 6:1 mol/mol) was also tested under the same conditions. The two catalysts were prepared and treated in the same manner, such that the only difference between the two materials was the support material (i.e., SiO$_2$ versus MWNTs). The rates and activation energies under product-free and full reformate gas conditions are shown in Figure 4. Nearly identical rates were measured on the two catalysts (Pt$_1$Na$_6$/1000-2h-C_N and Pt$_1$Na$_6$/SiO$_2$) under product-free WGS conditions. Under full reformate gas conditions, however, the WGS rate and E_{app} value deviated significantly on Pt$_1$Na$_6$/1000-2h-C_N, whereas they remained unchanged on Pt$_1$Na$_6$/SiO$_2$. We can interpret such a deviation in simple kinetic terms as a shift to a desorption-limited rate on the carbon-based catalyst, as discussed below.

It is well-known that hydrogen adsorption and spillover occur readily at high partial pressures of hydrogen on alkali-modified carbon nanotubes.[42,43] Silica, on the other hand, does not have any hydrogen storage capacity under these conditions. A series of hydrogen uptake experiments, shown in Figure 5
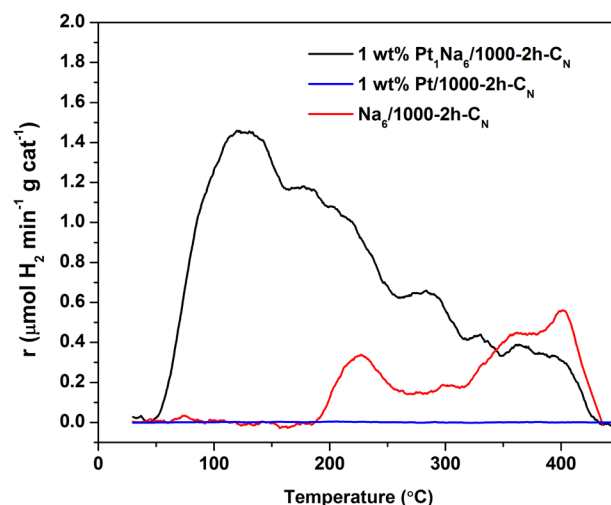

Figure 5. Temperature-programmed desorption of hydrogen from various MWNT-based materials. Reaction conditions: 30 mL/min He, 10 °C/min ramp rate. All materials were treated in 10% H$_2$ at 400 °C prior to the desorption study.

Table 1. Quantitation of Hydrogen Evolution from TPD Experiments[a]

catalyst	H$_2$ (μmol/g)
PtNa/1000-2h-C_N	28.3
Na/1000-2h-C_N	6.8
Pt/1000-2h-C_N	0.0

[a]As shown in Figure 5.

(quantified in Table 1), demonstrate the hydrogen storage capacity of the MWNTs in the presence of Pt and Na. It is particularly noteworthy that a 4-fold enhancement in hydrogen uptake was achieved on the Na-promoted Pt catalyst compared to the Na-doped, but Pt-free, MWNT support. Although hydrogen is generally known to have an inhibitory effect on the WGS reaction rate,[14,28,41] this is exacerbated on the carbon-supported catalyst because of the high hydrogen affinity of the catalyst surface.

The apparent reaction order with respect to hydrogen on the 1 wt % Pt$_1$Na$_6$/1000-2h-C_N catalyst was found to be lower (i.e., more inhibitory) than that reported for metal-oxide-supported materials[28] (see Figure S2, Supporting Information), further suggesting a higher surface hydrogen concentration. Furthermore, the adsorption of hydrogen onto such materials is an activated process; that is, the adsorption capacity increases with temperature.[44,45] In this light, we can attribute the inhibitory effect of hydrogen on 1 wt % Pt$_1$Na$_6$/1000-2h-C_N under the conditions used here to a H$_2$-desorption limitation. Indeed, previous studies have shown the hydrogen desorption energy from Pd-doped and annealed MWNTs to be as high as 130 kJ/mol,[46] in line with the increased apparent activation energy observed in Figure 4. This attenuation of the reaction rate was
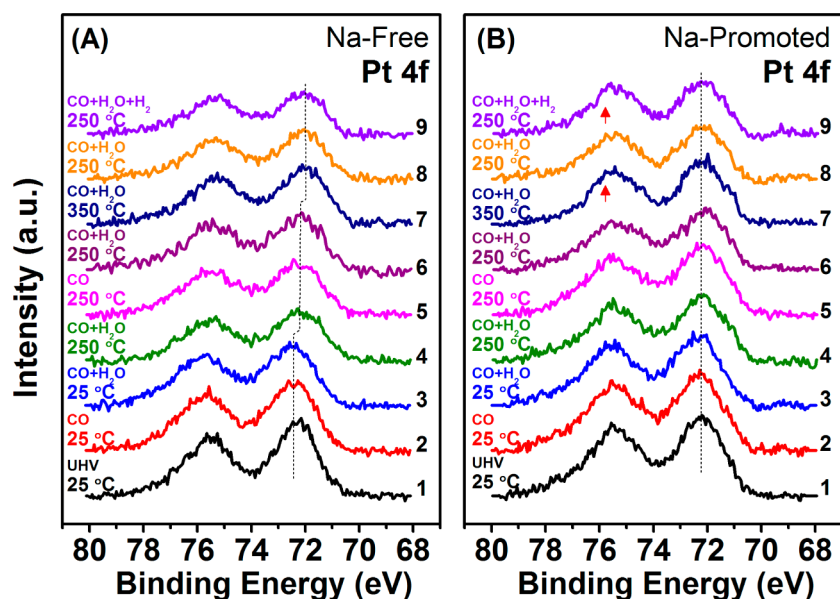
Figure 6. Pt 4f XP spectra of (A) Pt/1000-2h-C_N and (B) Pt$_1$Na$_6$/1000-2h-C_N under WGS reaction conditions.

observed to be reversible (by the removal of hydrogen), as shown in Figure S3 (Supporting Information) and in the XPS analysis below, indicating that the effect is not structural.

In Situ AP-XPS Studies. To better understand the response of the catalytic surface to the reaction conditions, AP-XPS experiments were conducted using the 1 wt % Pt$_1$Na$_6$/1000-2h-C_N and 1 wt % Pt/1000-2h-C_N catalysts. Acquisition of data was performed at steady-state conditions, after the samples had been held for 1 h at the conditions noted below. The catalysts were first examined by XPS under UHV conditions, after which the reactant gases (0.1 mbar of CO and 0.5 mbar of H_2O) were introduced sequentially at room temperature. The temperature was then increased to 250 °C under WGS reaction conditions (product-free gas feed). To probe the effect of a reducing atmosphere at elevated temperature, H_2O was removed from the gas phase and then reintroduced to test for the reversibility of the surface response. The stability of the catalyst was tested by increasing the temperature to 350 °C and then cycling back to 250 °C. Finally, to investigate the inhibitory effect of hydrogen, 0.5 mbar of H_2 was introduced in addition to the reactant gases (CO and H_2O) at 250 °C.

The Pt 4f signals for the Na-free (Pt/1000-2h-C_N) and Na-promoted (Pt$_1$Na$_6$/1000-2h-C_N) catalysts are shown in panels A and B, respectively, of Figure 6 (under various reaction conditions labeled 1−9). A close examination shows that the peak *shape* of the Pt$_1$Na$_6$/1000-2h-C_N signal (Figure 6B) is significantly more responsive to changes in the reaction atmosphere than the Na-free signal (Figure 6A), whereas the Pt 4f$_{7/2}$ and Pt 4f$_{5/2}$ peak *positions* (of Pt$_1$Na$_6$/1000-2h-C_N) remain constant. Conversely, the Pt 4f peak positions of Na-free Pt/1000-2h-C_N were observed to decrease in binding energy with reaction temperature, as indicated by the dotted line in Figure 6A. This is indicative of the progressive reduction of Pt with temperature under the reaction conditions. The lack of an overall shift of the Pt 4f peaks of Pt$_1$Na$_6$/1000-2h-C_N throughout the course of the reaction (Figure 6B) suggests that sodium is able to stabilize Pt in its active oxidation state.

The downshift of the Pt 4f signal for Pt/1000-2h-C_N along the reaction sequence was also consistent with the higher

propensity for sintering of Pt particles on the Na-free catalyst (Figure 3A) compared to Pt$_1$Na$_6$/1000-2h-C_N (Figure 3B). The aggregation of Pt nanoparticles on Pt/1000-2h-C_N decreased the fraction of low-coordinated Pt atoms dispersed on the MWNT surface, resulting in an increase of the metallic Pt signal at lower binding energies. The Pt atoms in Pt$_1$Na$_6$/1000-2h-C_N, on the other hand, are strongly bound to oxygen atoms within the Pt−Na$_x$−O$_y$−(OH)$_z$ complex, which contributes to their stabilization and prevents aggregation.

Deconvolution of the Pt 4f spectra of both Pt/1000-2h-C_N and Pt$_1$Na$_6$/1000-2h-C_N (Figure S4, Supporting Information) demonstrates the relative stability of the −OH groups on these surfaces, manifested as Pt−OH (i.e., Pt^{1+}) contributions. The change in intensity of the Pt−OH component over the course of reaction is shown in Figure 7 for both catalysts (with the
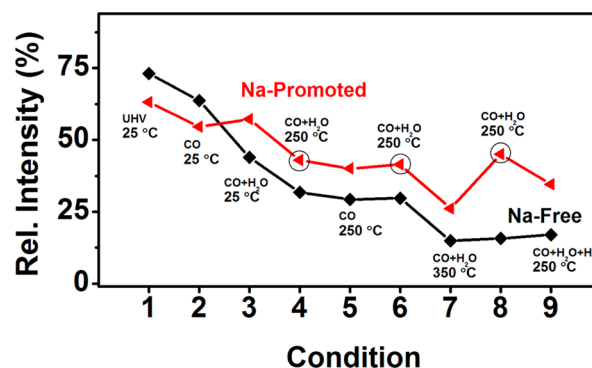

Figure 7. Pt−OH contributions to the Pt 4f signals of Pt$_1$Na$_6$/1000-2h-C_N (red) and Pt/1000-2h-C_N (black) over the course of the reaction. Circled points indicate benchmark reaction conditions (250 °C, 0.1 mbar of CO + 0.5 mbar of H_2O).

conditions on the *x* axis corresponding to the conditions numbered in Figure 6). For the Na-free sample, a progressive decrease in the relative intensity of the Pt−OH contribution as a function of temperature can be seen; two plateaus are observed (conditions 4−6 and 7−9) in Figure 7, corresponding
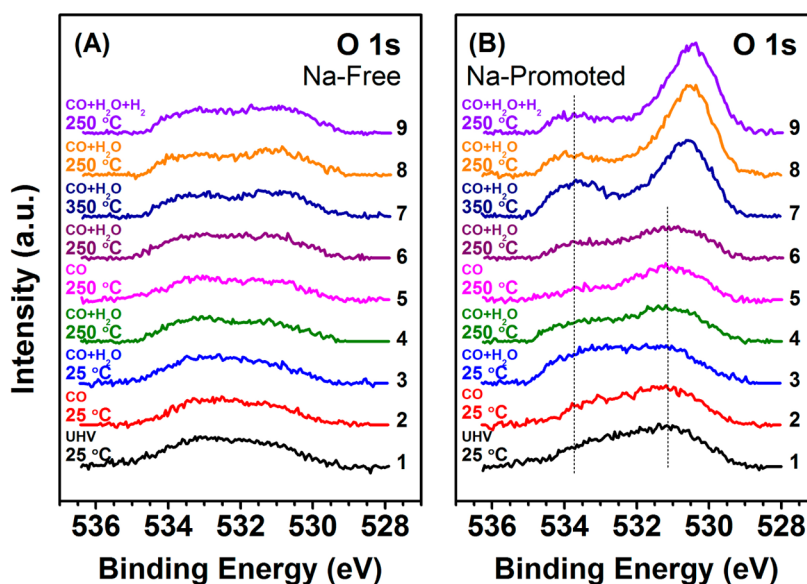
Figure 8. O 1s XP spectra of (A) Pt/1000-2h-C_N and (B) Pt$_1$Na$_6$/1000-2h-C_N under WGS reaction conditions.

to temperature increases (to 250 and 350 °C, respectively) that resulted in the agglomeration/reduction of Pt.

In contrast, the Na-promoted catalyst demonstrated a significantly higher contribution from the Pt−OH signal throughout the course of reaction. When the temperature was increased to 350 °C, where the WGS rate is very high and high surface coverages are not favored, this contribution dropped significantly (condition 7). Decreasing the temperature from 350 °C (condition 7) to 250 °C (condition 8) in the mixture of CO and H_2O resulted in a restoration of the Pt−OH signal intensity (condition 8). In fact the stability of this surface species (Pt−OH) at the benchmark reaction condition of 0.1 mbar of CO and 0.5 mbar of H_2O at 250 °C can be observed by the circled points in Figure 7, indicating the reversible response of the surface of Pt$_1$Na$_6$/1000-2h-C_N to varying conditions. The introduction of hydrogen (to the mixture of reactants CO and H_2O gas at 250 °C) in condition 9 of Figure 7 (corresponding to Figure 6B, condition 9) reduced the Pt−OH contribution. This indicates a decrease in the surface concentration of active sites, as corroborated by the kinetic data of Figure 4. Furthermore, the lack of response in the Pt−OH signal of the Na-free catalyst (Pt/1000-2h-C_N) demonstrates that Na contributes to the adsorption of −OH groups to Pt atoms.

The evolution of the O 1s photoemission features of the two catalysts, Pt/1000-2h-C_N and Pt$_1$Na$_6$/1000-2h-C_N, over reaction conditions 1−9 are shown in Figure 8. The contribution to O 1s from gas-phase CO (at ∼535.5 eV) was subtracted from the signal where appropriate. As shown in Figure 8A, the distribution of oxygen states for the Na-free catalyst appears to be relatively insensitive to the reaction conditions. This also corresponds to the observations for the Pt surface species shown in Figure 6A.

In contrast to the Na-free catalyst, the Pt$_1$Na$_6$/1000-2h-C_N catalyst exhibited significantly different O 1s photoemission features. Large surface changes were found to take place along the sequence of experimental conditions in Figure 8B. Compared to the Na-free catalyst (Figure 8A), for Pt$_1$Na$_6$/1000-2h-C_N, a significant contribution to the low-binding-energy (531.2 eV) side of the O 1s spectra is evident (Figure

8B). This binding energy is often attributed to surface hydroxyl surface species[47] and metal hydroxides.[48] We therefore assign the peak at 531.2 eV to the OH groups of the Pt−Na−O_x−(OH)$_y$ structure. The slight shift in this component under condition 5 (H_2O removed from the feed gas) is likely due to a high coverage of CO,[34,35] which was completely reversed upon the reintroduction of H_2O (condition 6), further demonstrating the stability of active −OH structure at these conditions.

Upon increasing the temperature to 350 °C under H_2O and CO pressure (Figure 8B, condition 7), the appearance of a strong new peak at 530.5 eV was observed. This new photoemission feature did not result from the shift of the peak at 531.2 eV, as the relative intensity of the peak at 530.5 eV to that at 533.8 eV increased significantly in conditions 7−9 (Figure 8B) compared to all previous conditions. The feature persisted on the surface even after the reaction temperature was again decreased to 250 °C (Figure 8B, condition 8) and after hydrogen was introduced into the gas phase (Figure 8B, condition 9). This component appears to be related to the enrichment of sodium on the surface, as shown in Figure 9.

The changes observed in the O 1s spectra are strongly reflected in the Na 1s signal shown in Figure 9. An upshift of the Na 1s binding energy upon increasing the temperature from 25 °C (Figure 9, condition 3) to 250 °C (Figure 9, condition 4) in the mixture of CO and H_2O was observed. This is likely the result of H_2O dissociation to OH, effectively oxidizing Na; that is, a transfer of electron density from Na to the adsorbed −OH group contributes to an upshift in the binding energy of Na 1s. Furthermore, the stability of the hydroxyl structure upon the removal of gas-phase water at 250 °C is apparent (condition 5). Indeed, these changes were also observed in the O 1s signal (Figure 8B).

The atomic ratio of Na to O at conditions 7−9 suggests that (1) the enrichment of sodium clearly takes place upon increasing the reaction temperature to 350 °C, corresponding to the appearance of the new O 1s features, and (2) this segregation of sodium is irreversible, as the atomic ratio Na to O remains nearly constant in conditions 8 and 9. This surface restructuring upon exposure to high temperatures might be responsible for the partial deactivation of Pt$_1$Na$_6$/1000-2h-C_N
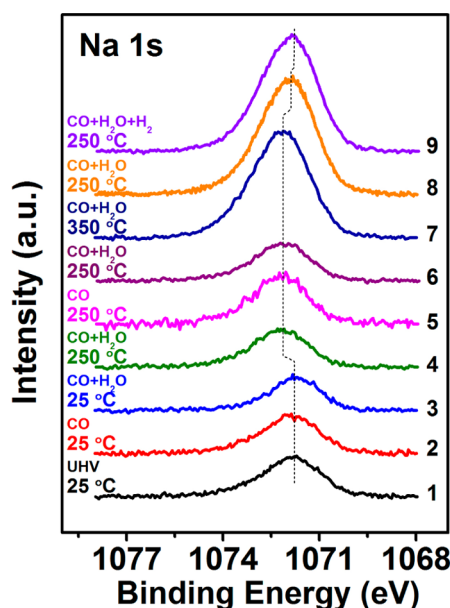
3243

dx.doi.org/10.1021/ja4123889 | *J. Am. Chem. Soc.* 2014, 136, 3238−3245

Figure 9. Na 1s XP spectra of $Pt_1Na_6/1000$-2h-C_N under WGS reaction conditions.

observed in the cooling cycle (Figure 1, arrow pointing from high to low temperature) by site blocking after exposure to WGS conditions at 400 °C. Thus, the in situ XPS studies rationalize both the activation of Pt by the presence of sodium and the partial deactivation of $Pt_1Na_6/1000$-2h-C_N catalyst after high-temperature exposure.

CONCLUSIONS

We have shown that the coimpregnation of Pt and Na onto a 1000 °C-annealed MWNT surface results in the formation of $Pt-Na_x-O_y-(OH)_z$ clusters. These subnanometer-sized active sites give rise to the observed WGS activity. In situ AP-XPS results show that, in the presence of Na, the $Pt-OH_x$ species are stabilized and the concentration of these species is a function of the gas-phase oxygen potential. Concomitantly, the reaction rate follows the changes in the $Pt-OH_x$ concentration. The stabilization of oxidized Pt by sodium and the ability of sodium to aid in the activation of water, even on carbon supports, is what gives rise to the high WGS activity on these catalysts. A strong inhibitory effect of hydrogen on these catalysts is explained by a (H_2) desorption-limited rate, as a strong uptake of hydrogen on the Pt−Na−carbon surfaces was measured above ∼200 °C.

ASSOCIATED CONTENT

S **Supporting Information**

Ex situ XPS of support materials, apparent reaction order results, reversibility of WGS rate with H_2 addition/removal, and deconvolution of AP-XPS spectra. This material is available free of charge via the Internet at http://pubs.acs.org.

AUTHOR INFORMATION

Corresponding Author

E-mail: maria.flytzani-stephanopoulos@tufts.edu

Notes

The authors declare no competing financial interest.

REFERENCES

(1) Gottesfeld, S.; Pafford, J. *J. Electrochem. Soc.* **1988**, *135*, 2651.
(2) Kušar, H.; Hočevar, S.; Levec, J. *Appl. Catal. B* **2006**, *63*, 194.
(3) Wang, X.; Rodriguez, J. A.; Hanson, J. C.; Gamarra, D.; Martínez-Arias, A.; Fernández-García, M. *J. Phys. Chem. B* **2006**, *110*, 428.
(4) Si, R.; Raitano, J.; Yi, N.; Zhang, L.; Chan, S.-W.; Flytzani-Stephanopoulos, M. *Catal. Today* **2012**, *180*, 68.
(5) Fu, Q.; Saltsburg, H.; Flytzani-Stephanopoulos, M. *Science* **2003**, *301*, 935.
(6) Pierre, D.; Deng, W.; Flytzani-Stephanopoulos, M. *Top. Catal.* **2007**, *46*, 363.
(7) Kwak, J. H.; Hu, J.; Mei, D.; Yi, C.-W.; Kim, D. H.; Peden, C. H. F.; Allard, L. F.; Szanyi, J. *Science* **2009**, *325*, 1670.
(8) Hatanaka, M.; Takahashi, N.; Tanabe, T.; Nagai, Y.; Dohmae, K.; Aoki, Y.; Yoshida, T.; Shinjoh, H. *Appl. Catal. B* **2010**, *99*, 336.
(9) Ruettinger, W.; Ilinich, O.; Farrauto, R. J. *J. Power Sources* **2003**, *118*, 61.
(10) Gorte, R. J.; Zhao, S. *Catal. Today* **2005**, *104*, 18.
(11) Trovarelli, A. *Catal. Rev.: Sci. Eng.* **1996**, *38*, 439.
(12) Ruettinger, W.; Liu, X.; Farrauto, R. J. *Appl. Catal. B* **2006**, *65*, 135.
(13) Deng, W.; Flytzani-Stephanopoulos, M. *Angew. Chem., Int. Ed.* **2006**, *45*, 2285.
(14) Grabow, L. C.; Gokhale, A. A.; Evans, S. T.; Dumesic, J. A.; Mavrikakis, M. *J. Phys. Chem. C* **2008**, *112*, 4608.
(15) Ratnasamy, C.; Wagner, J. P. *Catal. Rev.: Sci. Eng.* **2009**, *51*, 325.
(16) Flytzani-Stephanopoulos, M.; Gates, B. C. *Annu. Rev. Chem. Biomol. Eng.* **2012**, *3*, 545.
(17) Grenoble, D. C.; Estadt, M. M.; Ollis, D. F. *J. Catal.* **1981**, *67*, 90.
(18) Si, R.; Flytzani-Stephanopoulos, M. *Angew. Chem., Int. Ed.* **2008**, *47*, 2884.
(19) Hatanaka, M.; Takahashi, N.; Takahashi, N.; Tanabe, T.; Nagai, Y.; Suda, A.; Shinjoh, H. *J. Catal.* **2009**, *266*, 182.
(20) Fu, Q.; Deng, W.; Saltsburg, H.; Flytzani-Stephanopoulos, M. *Appl. Catal. B* **2005**, *56*, 57.
(21) Deng, W.; Frenkel, A. I.; Si, R.; Flytzani-Stephanopoulos, M. *J. Phys. Chem. C* **2008**, *112*, 12834.
(22) Deng, W.; Carpenter, C.; Yi, N.; Flytzani-Stephanopoulos, M. *Top. Catal.* **2007**, *44*, 199.
(23) Flytzani-Stephanopoulos, M.; Zhu, T.; Li, Y. *Catal. Today* **2000**, *62*, 145.
(24) Panagiotopoulou, P.; Kondarides, D. I. *J. Catal.* **2009**, *267*, 57.
(25) Zhu, X.; Hoang, T.; Lobban, L. L.; Mallinson, R. G. *Catal. Lett.* **2009**, *129*, 135.
(26) Pigos, J. M.; Brooks, C. J.; Jacobs, G.; Davis, B. H. *Appl. Catal. A* **2007**, *328*, 14.
(27) Zhai, Y.; Pierre, D.; Si, R.; Deng, W.; Ferrin, P.; Nilekar, A. U.; Peng, G.; Herron, J. A.; Bell, D. C.; Saltsburg, H.; Mavrikakis, M.; Flytzani-Stephanopoulos, M. *Science* **2010**, *329*, 1633.
(28) Pazmiño, J. H.; Shekhar, M.; Williams, W. D.; Akatay, M. C.; Miller, J. T.; Delgass, W. N.; Ribeiro, F. H. *J. Catal.* **2012**, *286*, 279.
(29) Wang, Y.; Zhai, Y.; Pierre, D.; Flytzani-Stephanopoulos, M. *Appl. Catal. B* **2012**, *127*, 342.
(30) Zugic, B.; Bell, D. C.; Flytzani-Stephanopoulos, M. *Appl. Catal. B* **2014**, *144*, 243.

(31) Tao, F.; Salmeron, M. *Science* **2011**, *331*, 171.

(32) Tao, F. F. *Chem. Commun.* **2012**, *48*, 3812.

(33) Shao, Y.; Yin, G.; Wang, J.; Gao, Y.; Shi, P. *J. Power Sources* **2006**, *161*, 47.

(34) Tao, F.; Dag, S.; Wang, L. W.; Liu, Z.; Butcher, D. R.; Bluhm, H.; Salmeron, M.; Somorjai, G. A. *Science* **2010**, *327*, 850.

(35) Björneholm, O.; Nilsson, A.; Tillborg, H.; Bennich, P.; Sandell, A.; Hernnäs, B.; Puglia, C.; Mårtensson, N. *Surf. Sci.* **1994**, *315*, L983.

(36) Vermang, B.; Juel, M.; Raaen, S. *Phys. Rev. B* **2006**, *73*, 033407.

(37) Stamatakis, M.; Chen, Y.; Vlachos, D. G. *J. Phys. Chem. C* **2011**, *115*, 24750.

(38) Pigos, J. M.; Brooks, C. J.; Jacobs, G.; Davis, B. H. *Appl. Catal. A* **2007**, *319*, 47.

(39) Bunluesin, T.; Gorte, R. J.; Graham, G. W. *Appl. Catal. B* **1998**, *15*, 107.

(40) Azzam, K.; Babich, I.; Seshan, K.; Lefferts, L. *J. Catal.* **2007**, *251*, 163.

(41) Phatak, A. A.; Koryabkina, N.; Rai, S.; Ratts, J. L.; Ruettinger, W.; Farrauto, R. J.; Blau, G. E.; Delgass, W. N.; Ribeiro, F. H. *Catal. Today* **2007**, *123*, 224.

(42) Wang, L.; Yang, R. T. *Energy Environ. Sci.* **2008**, *1*, 268.

(43) Wang, Z.; Yang, F. H.; Yang, R. T. *J. Phys. Chem. C* **2010**, *114*, 1601.

(44) Chen, P.; Wu, X.; Lin, J.; Tan, K. L. *Science* **1999**, *285*, 91.

(45) Yang, R. T. *Carbon* **2000**, *38*, 623.

(46) Yoo, E.; Gao, L.; Komatsu, T.; Yagai, N.; Arai, K.; Yamazaki, T.; Matsuishi, K.; Matsumoto, T.; Nakamura, J. *J. Phys. Chem. B* **2004**, *108*, 18903.

(47) Fisher, G. B.; Sexton, B. A. *Phys. Rev. Lett.* **1980**, *44*, 683.

(48) McIntyre, N. S.; Cook, M. G. *Anal. Chem.* **1975**, *47*, 2208.